

Investigation of the aquaporin-2 gating mechanism with molecular dynamics simulations

Hooman Hadidi¹  | Reza Kamali Ph.D., Professor¹  | Alireza Binesh²

¹Department of Mechanical Engineering, Shiraz University, Shiraz, Fars, Iran

²Hydro-Aerodynamics Division, Malek-e-Ashtar University of Technology, Shiraz, Tehran, Iran

Correspondence

Reza Kamali, Department of Mechanical Engineering, Shiraz University, Shiraz, Fars 71348-51154, Iran.
 Email: rkamali@shirazu.ac.ir

Abstract

Aquaporin-2 plays a vital role in the human kidney as a water passage channel. Any disorder with its function can cause water imbalance and consequently disease in humans, especially nephrogenic diabetes insipidus (NDI). For this reason, an accurate understanding of its performance can be useful for therapeutic purposes. In this article, we investigate the gating mechanism induced by spontaneous fluctuations in aquaporin-2's (AQP2) channels in the palmitoyl-oleoyl-phosphatidyl-ethanolamine lipid bilayer by molecular dynamics. Our results show that the selectivity filter (SF) in AQP2 is also a gating site depending on the side-chain conformation of His172. The important role of His172 in modulating the wide and narrow conformations has been further investigated by the simulation of the H172G mutant. The osmotic permeability values of all four monomers are in the range of wide state and the average is very close to that of the wide channel formed by wild-type AQP2. Moreover, by calculating the osmotic permeability and the potential of mean force of each of the AQP2 monomers for wide/narrow states of the SF, it is seen that the SF at its narrow conformation can induce a much larger energy barrier for water molecules permeation, hindering the transport of water molecules remarkably. The reason for the discrepancy among osmotic permeabilities of different monomers of aquaporins is revealed by investigating the osmotic permeability of each monomer through the wide/narrow states of their SF.

KEY WORDS

AQP2, gating mechanism, molecular dynamics, osmotic permeability, water transport

1 | INTRODUCTION

Aquaporins (AQPs) are a family of small membrane performing as semi-permeable conducting channels. The existence of AQPs is vital for the body's water homeostasis and control of the cell volume.¹ Water transports across cell membranes in two different ways, either by diffusion within the lipid bilayer or by translocation through AQPs. Water transport across biological membranes is improved within AQPs in response to osmotic pressure. The passage of water molecules across AQPs is known to be the fastest among biological processes, on a nanosecond timescale.² Some AQPs have also been found to conduct other small molecules and gases, such as ammonia,

carbon dioxide, and nitric oxide.^{3–5} Studies have reported that the inability of AQPs in water regulation may cause a number of diseases including obesity, diabetes insipidus, brain oedema, and cancer.^{6,7}

Since AQPs play an essential role in the water homeostasis of cells, their regulation is of great importance. Regulation can happen within trafficking or after translocation of the AQP to the cell's membrane. When the AQP is inserted in the membrane, channel gating occurs as an efficient regulatory mechanism facilitating a rapid response to external stimuli.⁸ AQPs have been proposed to be regulated by various mechanisms such as phosphorylation of serine residues, changes in divalent cation concentration, pH changes,⁹ applied membrane voltage, or membrane-mediated mechanical stress.⁸

Although the gating is controlled by an external factor, the intrinsic modes of AQP coupled to this process can be characterized by studying the spontaneous fluctuation induced by temperature.¹⁰

Human AQP2 plays a crucial role in the kidney, where it transports water within the apical membrane and is necessary for urine concentration.¹¹ Furthermore, regulation of water reabsorption which results in the body's water balance tuning can be done with AQP2 located mainly in the principal cells of the collecting ducts in the kidney. Experimental studies have revealed some conserved features of the AQP2 structure: Each AQP monomer is composed of six transmembrane alpha-helices with a central water-conducting channel, three extracellular and two cytoplasmic loops^{12,13} (as shown in Figure 1A). It is found that all of the monomers contain two conserved

Asn-Pro-Ala (NPA) motifs located in the middle of the water conduction pore acting as a constriction. There is another important constriction within the channel known as the aromatic/Arg (ar/R) selectivity filter (SF) located at the extracellular side of the pore and composed of a highly conserved arginine and an aromatic residue. It is now well known that the dysfunctionality of AQP2 plays a crucial role in nephrogenic diabetes insipidus (NDI).¹⁴

In recent years, computational methods have been developed to detect and analyze the translocation of water through biological channel proteins such as AQPs on a molecular level. Molecular dynamics (MD) simulations have emerged as the main computational tool for the study of biological processes such as water transport through AQPs.¹⁴ The difference between osmotic and diffusion permeabilities

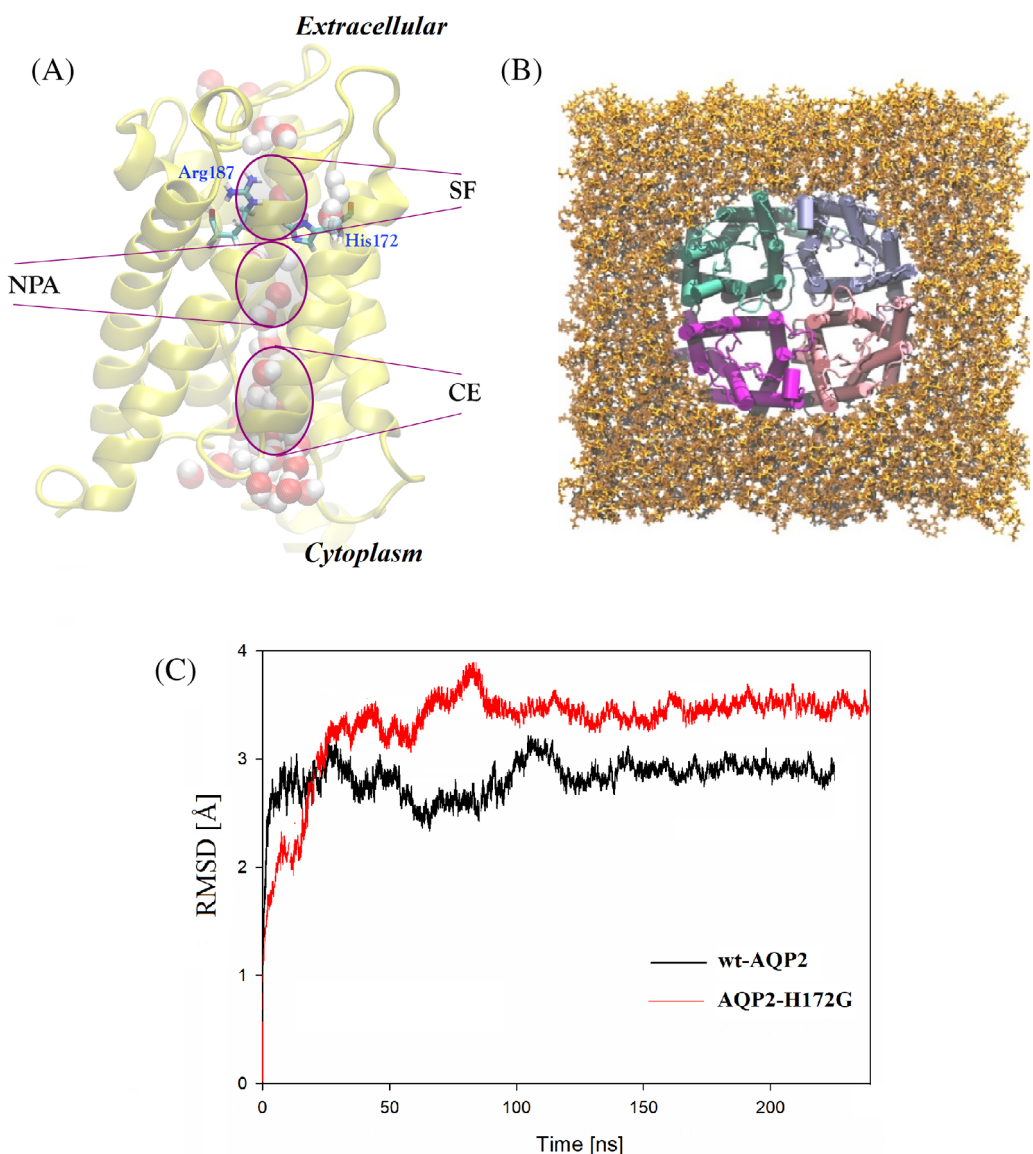


FIGURE 1 A, Lateral view of a monomer in wild-type aquaporin-2 (AQP2). Significant regions of a monomer as the ar/R selectivity filter (SF), NPA motif, and CE are indicated. B, Top view of the simulated system, including protein with four monomers and lipids. C, Root-mean-square deviations (RMSD) of wild-type AQP2 and AQP2-H172G with respect to the 4NEF crystal structure

of AQP1 was investigated by Zhu et al.¹⁵ in atomistic detail. It was revealed that the ratio of osmotic and diffusion permeabilities is related to the number of effective steps that a water molecule needs for permeating within a pore. In some studies, it was shown that AQPs preclude the permeation of protons; this has attracted the attention of many researchers in recent years. Hashido et al computed the water permeability of AQP1, AQPZ, AQPO, and GlpF employing MD simulations.¹⁶ According to their results, GlpF and AQPO had the largest and the smallest water permeabilities, respectively. Jensen and Mouritsen¹⁷ reported that their MD results show bigger water osmotic permeability for GlpF than AqpZ. Garate et al.¹⁸ calculated Human AQP4 water permeability in an MD study. It was shown that there is a discrepancy between theoretical and experimental permeabilities by a factor of about two.

In another MD study, AQPZ was studied by Xin et al.¹⁹ In their research, water permeation through this AQP was explored. It was revealed that there is a gating mechanism for water transport in this type of transmembrane proteins. Soon after the first molecular study by our group on AQP2 in which the diffusion permeability and osmotic permeability for water transport within AQP2's channels were obtained,¹⁴ Padhi et al examined some other issues including mechanism and energetics.²⁰ MD simulation has emerged as an important tool for exploring the gating mechanism in AQPs.^{10,18,21,22} In this regard, Janosi and Ceccarelli¹⁰ observed that the pores of AQP5 are closed because of different states of histidine in the CE region. Similar behavior was observed in AQP4.²²

In this work, the gating mechanism in wild-type AQP2 within the palmitoyl-oleoyl-phosphatidyl-ethanolamine (POPE) lipid bilayer is studied employing MD simulations.

It is shown that the ar/R region in AQP2 does not only act as a SF, which is already reported in the previous studies,^{14,20} but also acts as a gating site. Spontaneous fluctuations at the SF regions of the pores have been investigated and the conformational states of the His172 side chain have been related to the water permeation properties, in particular, key features such as diffuse and osmotic permeabilities and water occupancy.

Free energy profiles and hydrogen bond (H-bond) formation variations of the wide and narrow states have been obtained for different side-chain conformations of the aromatic residue His172, which provides strong support to the mechanism of gating through side-chain conformational change within the pores of AQP2 within POPE lipid bilayer.

Besides, by simulating the H172G mutation, the crucial role of His172 in regulating the water permeation is clarified. It is revealed that osmotic permeabilities of all four monomers are in the range of wide conformation and the average is very close to that of the wide state associated with the wild-type AQP2. Finally, the reason for the discrepancy among water permeabilities of AQPs monomers, reported in previous studies, was revealed by examination of the osmotic permeability of each monomer through the wide/narrow conformations of its SF. Our results may lead to the discovery of chemical modulators of AQP2 and the development of rational drug design for NDI treatment.

2 | MODELS AND METHODS

2.1 | Simulation details

In the present work, a high resolution (2.75 Å) X-ray crystal structure of the human AQP2 tetramer with PDB ID of 4NEF has been employed for the MD simulations.¹¹ To find optimal protonation states, ProteinPrepare²³ was utilized. It is a protein preparation web application that predicts the protonation states by computation of pK_a values for all of the titratable side chains. The calculations were based on pH = 7.4. Moreover, it calculates an optimal hydrogen bonding network of the protonated structures. In particular, based on the calculations it was found that the δ nitrogen of His172 is protonated, (ie it has been assigned as HSD). In order to build the simulation system, the AQP2's tetramer was embedded into a 120 × 120 Å² POPE lipid bilayers employing the Membrane Builder plugin of VMD software v1.9.3.²⁴ Afterward, AQP2 and POPE membrane were aligned and the lipid segments and water molecules were omitted in the range of 0.8 Å of the protein to avoid their probable overlap. Then, the protein and membrane were hydrated by adding water molecules layers of 18 Å thickness on the two sides of the system by using the Solvate plugin of VMD software. In the last step, the system was neutralized by adding Na⁺ and Cl⁻ ions with the 0.15 mol/L ionic concentration by using VMD's auto-ionize plugin. Figure 1B illustrates the entire system used in our MD simulations.

2.2 | MD setup

All the MD simulations are performed by employing the NAMD 2.13 simulation package,²⁵ The CHARMM36 force field was used for proteins and phospholipids.^{26,27} Besides, water molecules were modeled with the TIP3P model.²⁸ All of our simulations were carried out in an isothermal isobaric ensemble (1 atm, 310 K) by using the Langevin piston method and the Langevin dynamics thermostat with a Langevin damping coefficient γ = 5ps⁻¹.²⁹ Periodic boundary conditions were implemented to minimize the finite-size effects. Particle Mesh Ewald (PME) method³⁰ was employed to obtain long-range electrostatic interactions. Furthermore, computation of the van der Waals interactions was done by using a cut-off distance of 12 Å and a switching distance of 10 Å.

2.3 | MD simulation

Equilibrium MD simulation of the systems has been carried out in three steps. In the first step, the whole system except lipid tails was fixed to perform the minimization and equilibration of the lipid tails for 0.5 ns. To minimize the system in configuration space, minimization and equilibration of the system were done in the second step by applying harmonic restraints only to the protein atoms. In the last step, the systems without any restraint were equilibrated at constant temperature and pressure of 310 K and 1 atm, respectively.

2.4 | Water permeability analysis

To calculate water permeabilities, the continuous-time random walk (CTRW) model has been employed. This model, presented by Berezhkovskii and Hummer,³¹ is a known model used for studying water molecules translocation through biological pores.

According to the CTRW model, the single-channel diffusive permeability constant P_d can be obtained from equilibrium MD simulation as follows^{15,32}:

$$P_d = v_w \cdot q_0, \quad (1)$$

where v_w is the average volume of a single water molecule and q_0 is the number of water molecules crossing the channel per unit of time.

To calculate the osmotic permeability coefficient (P_f) from equilibrium MD simulations, the collective diffusion model proposed by Zhu et al³³ has been used. The normalized collective coordinate $n(t)$ can be computed based on the displacement of each water molecule through the channel in z-direction (dz_i) during the time step δt :

$$dn(t) = \sum_{i \in S(t)} dz_i / L(t), \quad (2)$$

$$n(t) = \int dt / L(t) \sum_{i \in S(t)} [z_i(t) - z_i(t - \delta t)], \quad \delta t = 2ps, \quad (3)$$

where δt represents the time step size. $S(t)$ indicates the set of translocating water molecules in the pore. The constriction region length $L(t)$ for each pore is defined as the distance along the z-axis of the SF residue Arg187's geometric center and the oxygen atom of Gly64^{17,18}; It represents the pore lumen exhibiting single-file water transport in the relatively flexible channels of AQP2. This length was obtained every 2 ps, yielding an average value of $L(t) \approx 19.2 \text{ \AA}$.

The collective diffusion constant can be computed by the following Equation¹⁴:

$$D_n = \langle n^2(t) \rangle / 2t, \quad (4)$$

where $\langle n^2(t) \rangle$ indicates the mean square displacement (MSD) of $n(t)$. Then, the osmotic permeability (P_f) can be computed by:

$$P_f = v_w D_n. \quad (5)$$

To calculate the osmotic permeability obtained from Equation (5), the MSD was calculated using a time-window of 50 ps, (see Equation (4)); therefore, for instance, for a 10 ns duration simulation, the calculated permeability represents an average of 200 values.

2.5 | Calculation of the potential of mean force (PMF)

The potential of mean force (PMF) was calculated within the pores by dividing the channel into zones of 2 Å and then computing the

average water density $\rho(z)$ in each region. The PMF can be obtained as follows³⁴:

$$\text{PMF}(z) = -KT \ln \left[\frac{\rho(z)}{\rho_{\text{bulk}}} \right], \quad (6)$$

where K , ρ_{bulk} and T represent the Boltzmann constant, the bulk density, and the absolute temperature, respectively.

3 | RESULTS AND DISCUSSION

3.1 | RMSD profile of AQP2

The evaluation of the simulation stability was carried out by calculating the RMSD of the protein backbone atomic coordinates relative to those of the initial structure, as shown in Figure 1C. The conformation of wt-AQP2 has reached reasonable stability after 125 ns, and the RMSD values converge to $\sim 2.9 \text{ \AA}$. Therefore, the last 100 ns of this simulation were chosen for data analysis.

3.2 | Conformational changes of SF as wide/narrow

To investigate the structural changes of the protein pores at specific time points during the MD simulation time, measurement of the minimum distances between the residues constructing the pores at these time points has been performed by using a home-made python-based code.

First, by visual inspection, it was detected that His172 alters the diameter of the pore at the SF.

To examine the gating mechanism of AQP2 in the SF region, the local constriction indicator (D) has been introduced as the distance between NE2 nitrogen atom of His172 and NE nitrogen atom of Arg187 at the SF region. As can be observed in Figure 2, the local constriction indicator in the SF region varies from about 8 Å in the wide conformation allowing the passage of water molecules to about 4 Å in the narrow conformation, where residues of Arg187 and His172 are located close to each other and significantly restrict the transport of water molecules. Another conformation (semi-narrow) can be observed in monomer C populated at values approximately between 5 and 6.5 Å, which is an unstable state. Noteworthy, it was detected that the possibility of wide/narrow states and their durations varies in four monomers, such that monomer-3 has the longest duration of narrow conformation and monomer-2 has the shortest.

Furthermore, by plotting the N-CA-CB-CG dihedral angle of His172 (Figure 3), a direct relation between diminishing the channel pore diameter and rotation of His172 was revealed. As can be seen, when a wide to narrow state transition occurs for the SF region, this dihedral angle changes from an average $\sim -150^\circ$ to $\sim -70^\circ$ in the four monomers.

A close view of the changes in SF conformations can also be seen in Figure 4A,B. Variations in the size of the channel pore diameter are

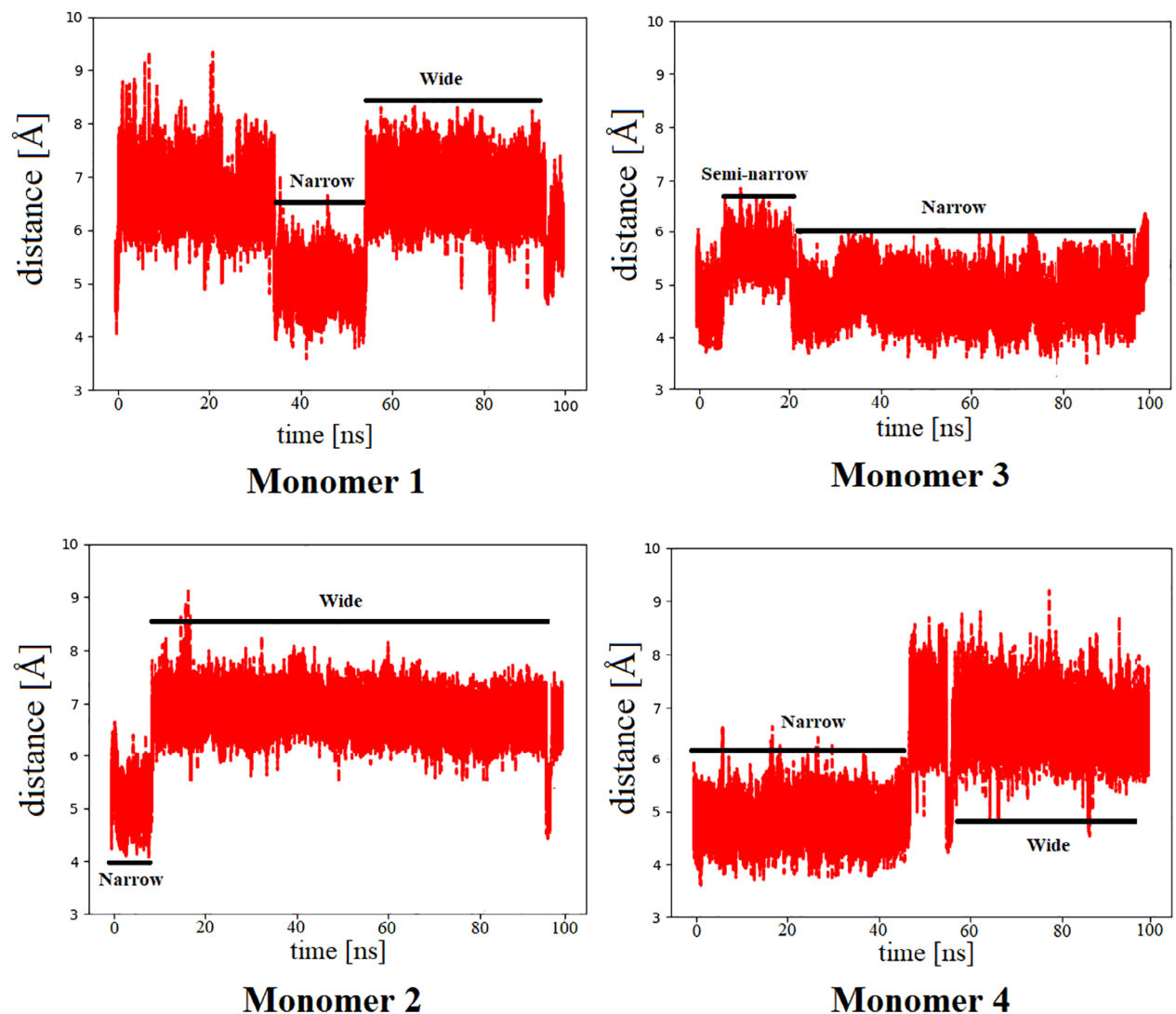


FIGURE 2 Variations of the distance between the NE2 nitrogen atom of His172 and NE nitrogen atom of Arg187 at the selectivity filter (SF) region during 100 ns of simulation indicating transitions between wide, narrow, and semi-narrow conformations for four monomers of wild-type aquaporin-2 (AQP2) [Color figure can be viewed at wileyonlinelibrary.com]

because of both displacement and rotation of His172's ring toward the channel, such that this ring protrudes into the channel and limits the water molecules transport. The white dotted lines in the figure with VMD's analysis tool, RIP-MD represent the hydrogen bonds (H-bonds) among atoms of His172 and those of adjacent residues plotted.³⁵ As illustrated, the hydrogen bond between NE2 nitrogen atom of His172 and HG1 hydrogen atom of Cys181 has been detected to be stably maintained in the narrow conformation of SF but is missing from the wide state. This is also observable in Figure 5 showing the frequency of H-bond formations between the above-mentioned atoms. In this figure, the number of H-bonds formed between NE2 nitrogen atom of His172 and HG1 hydrogen atom of Cys181 in the time windows of 4 ns is indicated.

In reference 20, with the monomeric simulation of AQP2, conformational change of an AQP2 ar/R SF residue, Phe48, was reported. While, in the present work, in which tetrameric configuration of

AQP2 has been simulated, it is observed that similar to AQP4²² and AQP5,¹⁰ histidine plays the main role of gating in the SF region. These different findings of the key residue in the SF region with conformational transitions can be due to the different configurations employed in the simulations. Janosi et al.¹⁰ performed both monomeric and tetrameric simulations of AQP5 and they found that "the tetrameric configuration, that is, the protein-protein coupling, is mandatory for the correct functioning of the gating mechanism.", since with the monomeric simulation of the AQP, there is a possibility of eliminating the lateral forces that are present in the tetrameric assembly and they can be necessary for correct simulation of the gating function.

Moreover, the usage of different lipid bilayers (POPE in our work against POPC in reference 20) may affect conformational mobility of the residues. Since the POPC head group is significantly bulkier than the POPE head group,^{17,36,37} it can impose different stress on the structure of AQP2.

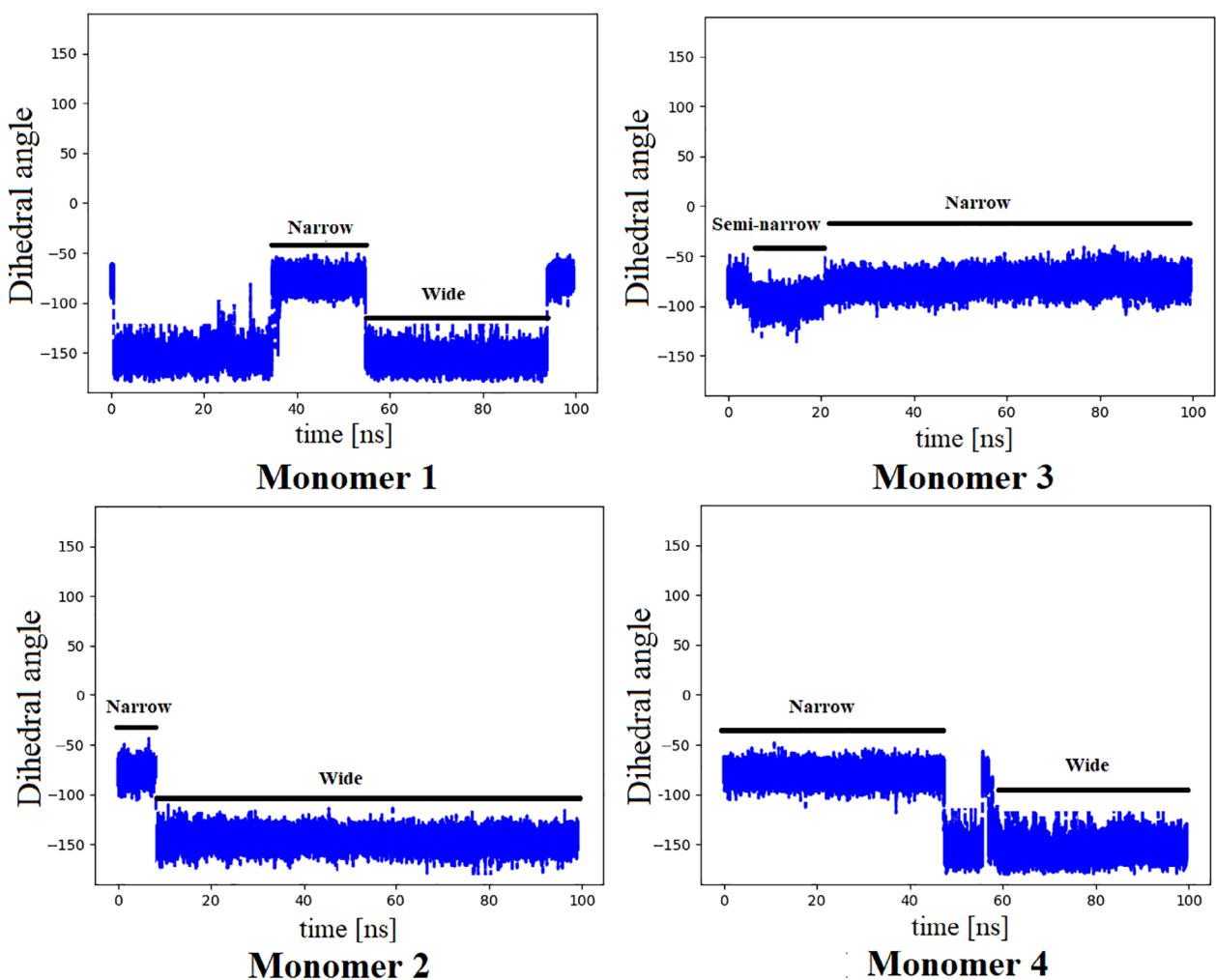


FIGURE 3 Variations of the His172 dihedral angle (N-CA-CB-CG) for four monomers of wild-type aquaporin-2 (AQP2) during 100 ns of simulation causing transitions between wide and narrow states in the selectivity filter [Color figure can be viewed at wileyonlinelibrary.com]

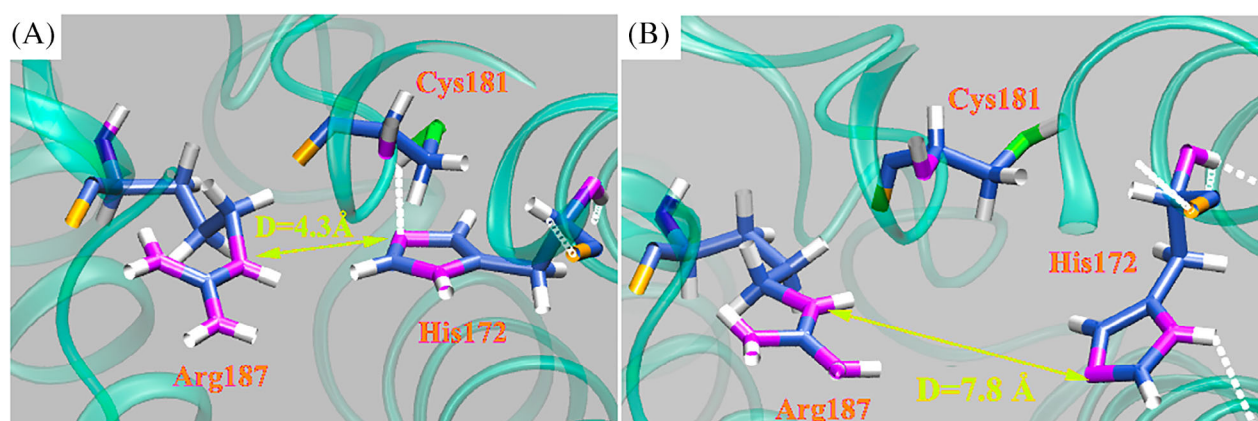


FIGURE 4 Close view of the distance between NE2 nitrogen atom of His172 and NE nitrogen atom of Arg187 at the selectivity filter (SF) region of wild-type aquaporin-2 (AQP2) for A, narrow and B, wide conformations. There is a stable hydrogen bond between NE2 nitrogen atom of His172 and HG1 hydrogen atom of Cys181 in the narrow state of SF but is missing from the wide state. The white dotted lines show the hydrogen bonds among atoms of His172 and those of adjacent residues [Color figure can be viewed at wileyonlinelibrary.com]

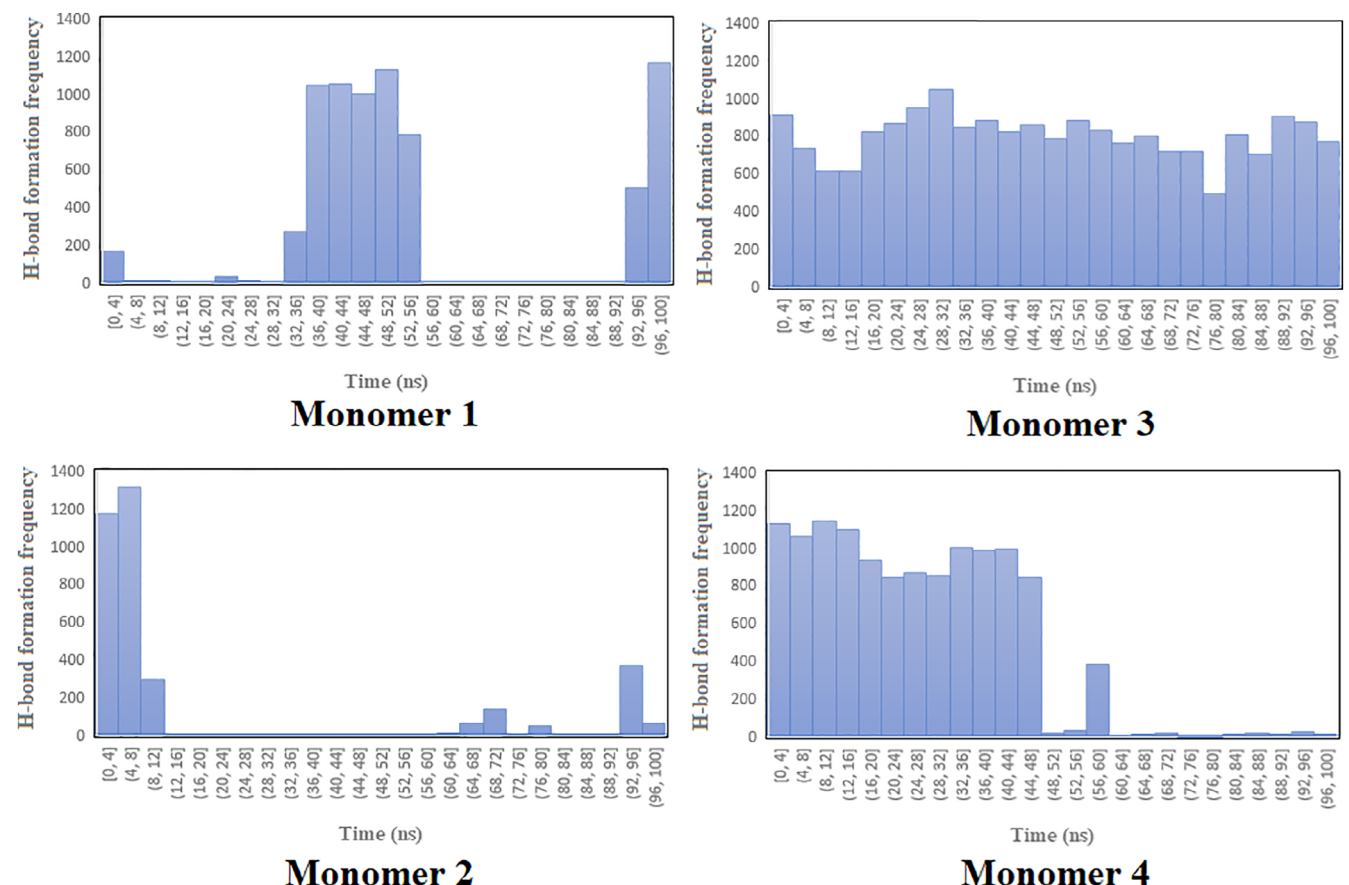
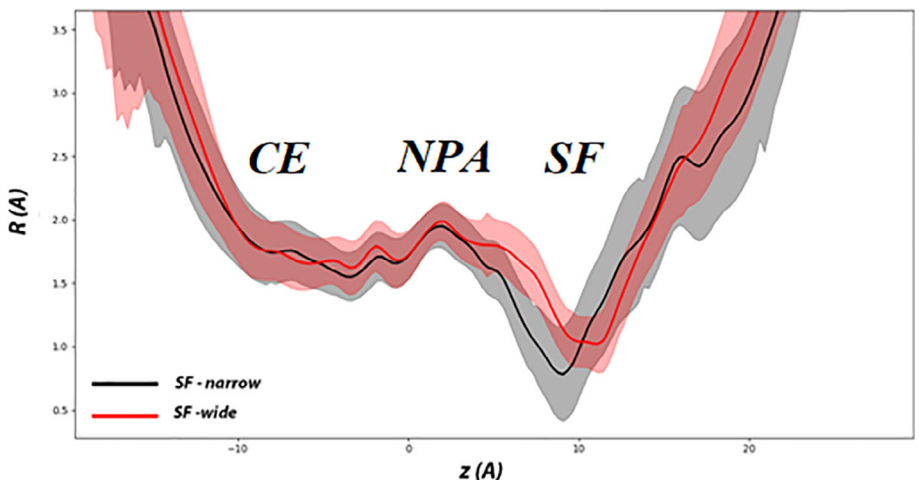


FIGURE 5 Histograms of the H-bond formation frequency between NE2 nitrogen atom of His172 and HG1 hydrogen atom of Cys181 in the four monomers of wild-type aquaporin-2 (AQP2) [Color figure can be viewed at wileyonlinelibrary.com]

FIGURE 6 Comparison of the average pore radius profiles (R) along the pore axis (z) for narrow and wide states of the selectivity filter in wild-type aquaporin-2 (AQP2). The profiles have been averaged for 100 ns molecular dynamics (MD) simulation. The shadows are indicators of the SD [Color figure can be viewed at wileyonlinelibrary.com]



3.3 | Radius profiles of the pores

The average radius profiles have been plotted in Figure 6 by using HOLE 2³⁸ for these two conformations: Wide conformation with smallest radii mostly above 1 Å which is shown with a red line and narrow conformation illustrated with a gray line. Distribution of the radius profile shows that the channel at the SF region in the narrow

conformation can be constricted to approximately 1 Å making the passage of water molecules very difficult. Our calculated smallest radii corresponding to wide and narrow conformations of the SF region match well with those of references 10, 22.

We also examined the CE region in AQP2 to see if a closed conformation can be detected in the cytoplasmic region similar to the behavior reported for AQP4 and AQP5.^{10,22} However, with a visual

inspection, no such closure was seen for the simulation of AQP-2 during 100 ns. Besides, it is also observable from the radius profile plotted with SD (Figure 6) that the pore radius in the CE region ($-11 < z < -7$) does not drop below 1.5 Å, which means that this region can be considered as always open.¹⁰

Furthermore, similar to AQP4²² and AQP5,¹⁰ it is found that the radius of the NPA region is almost constant during simulations and does not transform between different states. In other words, this region only acts as a filter in AQP2, not gating.

3.4 | Calculation of the free energy profiles for wide/narrow states of the SF

The PMF profiles as a function of position along pore axis (z) for four monomers of the AQP2 have been obtained for time intervals corresponding to wide/narrow conformations (Figure 7). As can be

seen in this figure, the three monomers 1, 2, and 4 have different values of PMF within the SF region for its wide and narrow states. For every PMF profile reported in this work, the convergence is checked via the block averaging method³⁹ to make sure that the duration time for PMF computation of water transport associating with the different conformations of the monomers is long enough to obtain accurate profiles. For instance, the convergence plots of monomer 1 corresponding to wide and narrow conformations are illustrated in Figure S1. The uncertainty related to the main barriers was calculated as less than 0.25 kcal/mol. The free energy barrier of the SF region against water molecules transport for the wide conformation in monomers 1, 2, and 4 is as low as 1.5 kcal/mol. This is similar to the value of about 1.3 kcal/mol obtained for SF's energy barrier within one of the monomers averaged over the total MD trajectory in reference 20, probably corresponding to a mostly wide conformation of the SF region. This low energy barrier permits the rapid passage of water molecules. However, for the narrow conformation of SF, the SF's

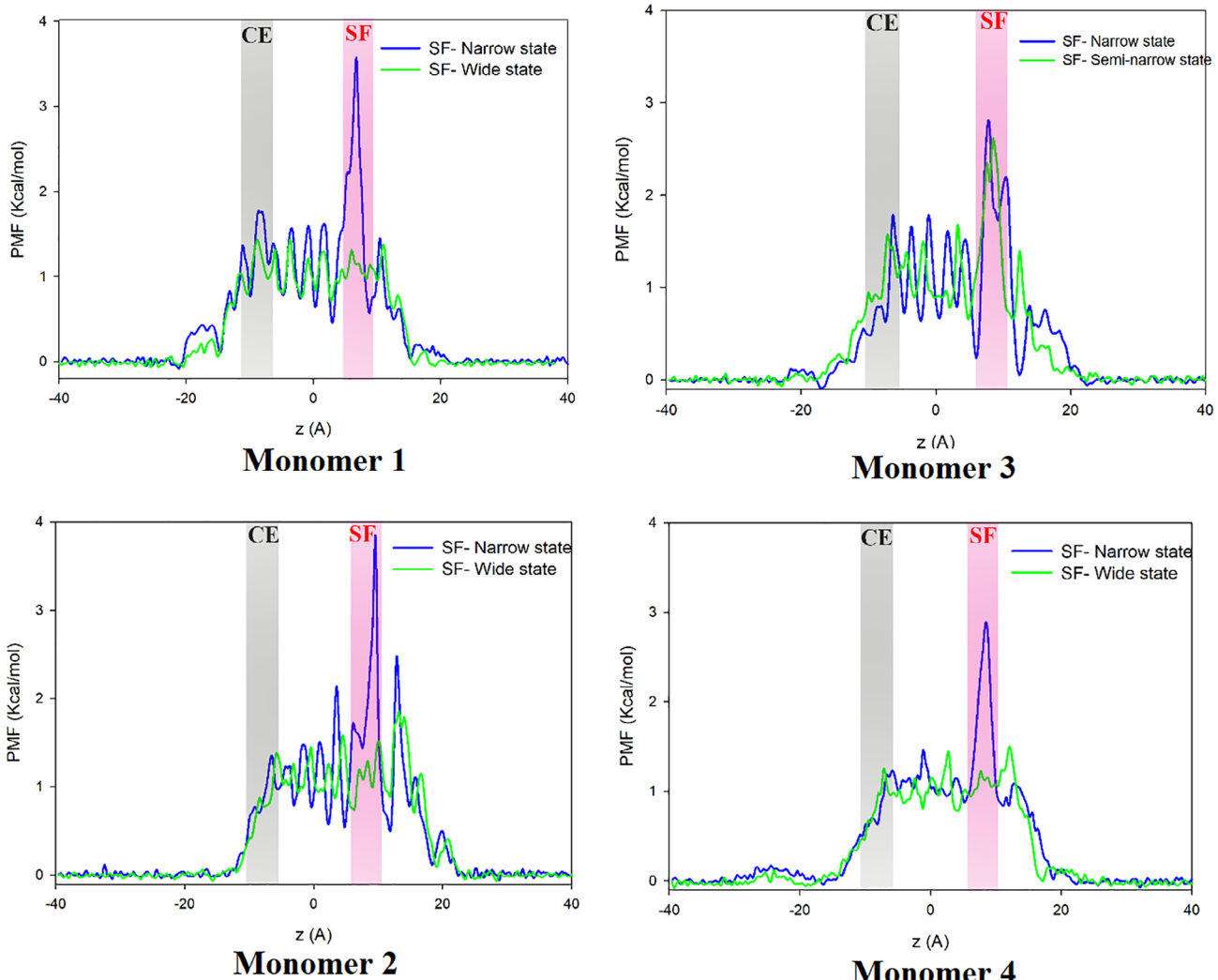


FIGURE 7 Potential of mean force (PMF) profiles of water molecules permeation as a function of position along pore axis (z) through different monomers for wide/narrow conformations of the selectivity filter (SF) in wild-type aquaporin-2 (AQP2) [Color figure can be viewed at wileyonlinelibrary.com]

energy barrier in these monomers gets close to 3.4, 3.8, and 2.7 kcal/mol, respectively. For monomer 3, the SF region was found to be narrow or semi-narrow, given that in the 100 ns interval, His172 and Arg187 in SF are relatively close apart and no wide conformation could be observed. Consequently, the free energy barrier changes in the SF region in narrow or semi-narrow states do not make much difference for this monomer. In addition, from the free energy plots, it can be observed that the free energy barrier corresponding to the CE region in any of the monomers does not exceed 1.5 kcal/mol relating to the open conformation of the CE region that water molecules can easily pass through.²²

In AQP4²² and AQP5,¹⁰ the main role of the gating mechanism is played by the CE region, so that for relatively long periods of time, even up to 100 ns, it was observed that it could remain closed. But such behavior did not exist in the SF region and its closure was much less persistent. According to our observations, no gating behavior was detected in the CE region of AQP2 at all, and it was the SF region whose conformational transition remarkably affected the permeability of the pore.

3.5 | Water transport properties of AQP2

Here, the effect of wide/narrow states of the pores on the water transport properties is investigated. Table 1 shows the osmotic permeability (P_f) for wide/narrow states and also for total production simulation time.

Although different lipid bilayers have been used in the present MD simulation (POPE) and reference 20 (POPC), our computed P_f averaged over the entire MD product simulation time ($9.89 \pm 4.03 \times 10^{-14} \text{ cm}^3/\text{s}$) matches well with that of reference 20 ($10.9 \pm 1.6 \times 10^{-14} \text{ cm}^3/\text{s}$). It means that P_f does not significantly depend on the lipid headgroup, which is consistent with the findings of reference 17 in which carried out MD simulations on AQPZ and GlpF with POPC and POPE lipid bilayers.

TABLE 1 Osmotic permeability (P_f) for different monomers of wt-AQP2 and AQP2-H172G mutant

	Monomer 1	Monomer 2	Monomer 3	Monomer 4	Mean \pm SD
P_f of wt-AQP2 (Averaged over SF-wide state)	14.65	14.08	—	13.56	14.09 ± 0.44
P_f of wt-AQP2 (Averaged over SF-narrow state)	6.41	6.28	3.44	4.17	5.07 ± 1.29
P_f of wt-AQP2 (Averaged over total production simulation time)	13.53	14.15	4.82	7.08	9.89 ± 4.03
P_f of AQP2-H172G (Averaged over total production simulation time)	14.14	13.14	14.05	13.72	13.76 ± 0.39

Abbreviations: AQP2, aquaporin-2; SF, selectivity filter.

TABLE 2 Diffusive permeability (P_d) in units of $10^{-14} \text{ cm}^3/\text{s}$ for different monomers of wild-type AQP2

	Monomer 1	Monomer 2	Monomer 3	Monomer 4	Mean \pm SD
P_d (Averaged over SF-wide state)	1.54	1.41	—	1.86	1.60 ± 0.19
P_d (Averaged over SF-narrow state)	0.47	0.35	0.14	0.31	0.32 ± 0.12
P_d (Averaged over total production simulation time)	1.03	1.12	0.18	0.98	0.82 ± 0.38

Abbreviations: AQP2, aquaporin-2; SF, selectivity filter.

Besides, it is interesting to see that the calculated osmotic permeability in the narrow state of SF, that is, $5.07 \pm 1.29 \times 10^{-14} \text{ cm}^3/\text{s}$, is in good agreement with the experimental value of $P_f^{\text{exp}} \sim 3.3 \pm 0.2 \times 10^{-14} \text{ cm}^3/\text{s}$.⁴⁰ This might be due to the experimental conditions likely keeping the SF region in the narrow state. As mentioned in the introduction, there are various external factors which can play a critical role in the gating of AQPs. In particular, it is found that the constriction region of the AQPs can be closed by adding divalent cations or lowering the pH.⁸

As can be seen in Table 1, water transport occurs even when the SF region is at its narrow conformation. However, the water molecules pass at much lower rates in comparison with the wide state. Moreover, the average osmotic permeability of the monomers for the entire production simulation time is calculated with a large difference from $4.82 \times 10^{-14} \text{ cm}^3/\text{s}$ (in monomer 3) to $14.15 \times 10^{-14} \text{ cm}^3/\text{s}$ (in monomer 2). But when we compare P_f of the monomers for the wide state of the SF, the negligible difference among them can be observed. These results confirm similar behavior of water passing through each monomer and different time evolution of each monomer.

It should be noted that, as can be seen in Table 1, there is still a relatively notable difference among the permeability values associated with the narrow state of the SF region. A possible explanation for such variance might be the deviation of the pores from the concerted single-file water transportation in this conformation of the SF, which is discussed in the following paragraph. Nevertheless, the variance among P_f values of the four monomers associated with the wide/narrow states (with SDs of ± 1.29 and ± 0.44 , respectively) is significantly smaller than that corresponding to the average values (with the SD of ± 4.03).

The values of P_d , P_f/P_d , and N are also summarized in Tables 2–4. In the idealized single-file water transportation, the continuous-time random walk model¹⁵ predicts that $P_f/P_d = N + 1$, where N is the average number of water molecules occupying the pore. As can be seen in

TABLE 3 The ratio of P_f/P_d for different monomers of wild-type AQP2

	Monomer 1	Monomer 2	Monomer 3	Monomer 4	Mean \pm SD
P_f/P_d (Averaged over SF-wide state)	9.51	9.98	—	7.29	8.93 ± 1.17
P_f/P_d (Averaged over SF-narrow state)	13.64	17.94	24.64	13.48	17.43 ± 4.53
P_f/P_d (Averaged over total production simulation time)	9.96	11.27	20.95	8.32	12.63 ± 4.92

Abbreviations: AQP2, aquaporin-2; SF, selectivity filter.

TABLE 4 The average number of permeated water molecules for different monomers of wild-type AQP2

	Monomer 1	Monomer 2	Monomer 3	Monomer 4	Mean \pm SD
N (Averaged over SF-wide state)	6.48	6.71	—	6.13	6.44 ± 0.24
N (Averaged over SF-narrow state)	3.47	6.47	7.39	4.32	5.41 ± 1.58
N (Averaged over total production simulation time)	5.47	6.32	6.28	5.42	5.87 ± 0.43

Abbreviation: AQP2, aquaporin-2; SF, selectivity filter.

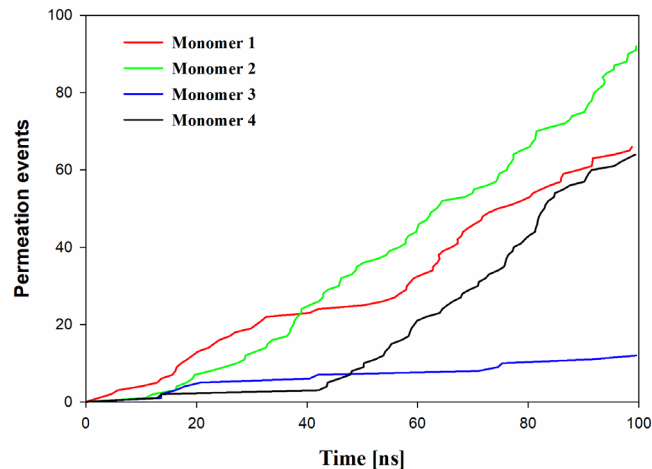
**FIGURE 8** Cumulative permeation events in both directions of the wild-type aquaporin-2 (AQP2) pores during the molecular dynamics (MD) production simulation time [Color figure can be viewed at wileyonlinelibrary.com]

Table 3 and Table 4, for wide conformation of the SF region, the P_f/P_d ratio is close to $N + 1$. However, for the narrow state, because of the extremely low P_d , the P_f/P_d ratio turns out to be larger values suggesting that wide channels provide nearly idealized single-file water transportation while narrow pores do not.

Figure 8 depicts the cumulative permeation events in both directions of the pores during the MD production simulation time. As can be observed, the highest permeation rates correspond to the wide conformations of the SF region in the monomers (see Figure 2), while low permeation rates are associated with the narrow conformations. These low permeation rates can be seen in the time periods of approximately 35–55, 0–10, and 0–45 ns of monomers 1, 2, and 4, respectively. Monomer 3 has the smallest total permeation rate with mostly narrow conformation during the MD trajectory time.

Furthermore, MD simulation has been carried out on the H172G mutant supporting the great relevance of such residue in SF gating. As can be seen in Figure 1C, the RMSD values of AQP2-H172G, with

remarkably higher oscillations compared to the wild-type AQP2, converge to ~ 3.5 Å. To make sure that the atoms of this system have reached reasonable stability, the last 140 ns have been selected for data production. The time evolution of the local constriction indicator is shown in Figure 9. As can be seen in this figure, the analysis of the 140 ns trajectory indicates that upon replacement of His172 with glycine, the SF narrowing has not been observed in any of the four monomers, which confirms the key role in the proposed gating mechanism of the histidine residue in the SF region. For the wild-type AQP2, 140 ns of the simulation were sufficient to observe the SF closure in the monomers (see Figure 2), while the time evolution of four monomers in AQP2-H172G displays only the wide conformation for the SF region.

Moreover, the calculation of the osmotic permeability for the AQP2-H172G mutant, confirms our observations (as shown in the last row of Table 1). The computed value (averaged over the four monomers) is equal to $13.76 \pm 0.39 \times 10^{-14}$ cm³/s, fully comparable to that obtained for the wide conformation of wild-type AQP2 ($14.09 \pm 0.44 \times 10^{-14}$ cm³/s).

4 | CONCLUSION

In the present study, the gating mechanism within AQP2 in the POPE lipid bilayer has been investigated. The main objective of this study was to determine the structural dynamics of AQP2's channels to understand the gating mechanism in AQP2, comprehensively. The conformational changes in the SF region of AQP2 were examined in our work by analyzing the minimum distances between residues in this region and by plotting the variations of radius profiles, H-bond formation, permeation events, and PMF profiles of water molecules transport during 100 ns MD production simulation time of AQP2.

In the previous studies of AQP4²² and AQP5,¹⁰ it was observed that the main rate-limiting zone for these AQPs is located in the CE region of the pore. The narrow conformation of the SF occurred at

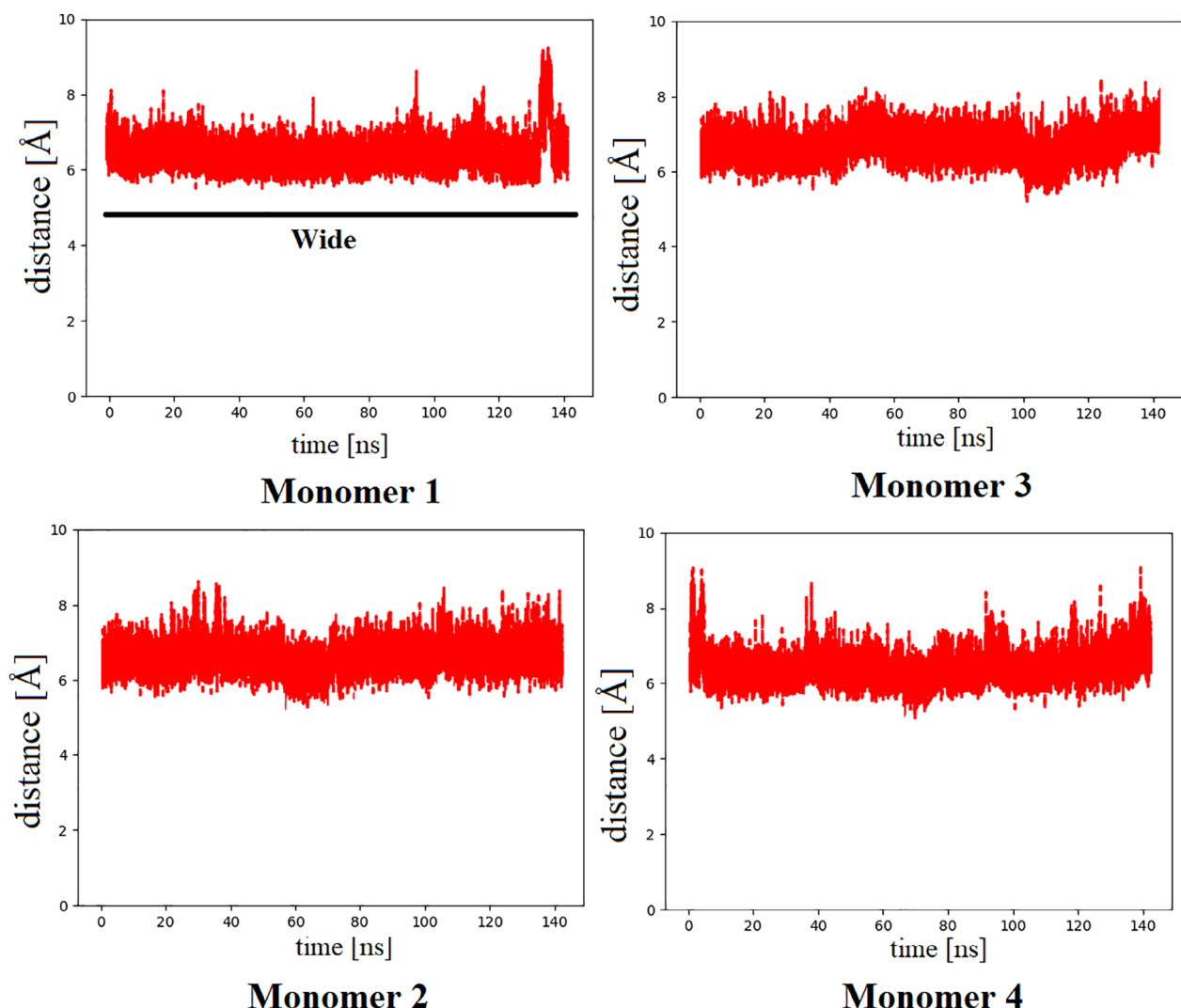


FIGURE 9 Variations of the distance between carbon alpha atom of Gly172 and NE nitrogen atom of Arg187 at the selectivity filter (SF) region of aquaporin-2 (AQP2)-H172G during 140 ns of simulation [Color figure can be viewed at wileyonlinelibrary.com]

low probability and, when it happened, it lasted for a few nanoseconds. On the contrary, we have found that in AQP2, the SF is the only region that regulates the water translocation through the pores.

Our results showed that the SF region in AQP2 switches between narrow and wide states. The aromatic residue His172 plays the main role in the gating mechanism due to its ring orientation and approaching Arg187. As a result, the channel radius becomes narrower and impedes water molecules transport through the pore. Furthermore, by inspecting the radius profile and free energy profiles of the AQP2, it was revealed that the channel radius in the CE region does not become lower than 1.5 Å and with the maximum energy barrier of 1.5 kcal/mol, it can be considered as open.

Free energy profiles of each of the AQP2 monomers confirmed the effect of the SF transition between wide/narrow states, such that the free energy barrier of the SF region for the wide state in three monomers was calculated to be about 1.5 kcal/mol. But for the narrow state of the SF, the free energy barrier peaks of 2.7 to 3.8 kcal/mol were observed for the monomers of AQP2, hindering the passage of water molecules.

mol were observed for the monomers of AQP2, hindering the passage of water molecules.

The important role of His172 in modulating the wide and narrow conformations has been further explored by the simulation of the H172G mutant. It was shown that the osmotic permeability values of all four monomers are in the range of wide conformation and the average is very close to that of the wide channel formed by AQP2 wild-type.

Furthermore, the cause of the large difference among osmotic permeabilities of different monomers was examined by investigating the osmotic permeability of each monomer through the wide/narrow states of their SF. It was found that although the average osmotic permeabilities of the monomers for the entire equilibrium time have a large difference, calculated from $4.82 \times 10^{-14} \text{ cm}^3/\text{s}$ (in monomer 3) to $14.15 \times 10^{-14} \text{ cm}^3/\text{s}$ (in monomer 2). But by comparing the osmotic permeabilities of the monomers for wide states of the SF, a negligible difference among them can be seen. These results confirm similar behavior of water passing through each monomer and different time evolution of each one.

In the end, it should be noted that the limited length of the MD simulations in this study is a potential source of error that may affect some results, in particular, in determining the accurate population distribution of wide/narrow conformations and calculation of average water permeability values. However, a fully atomistic MD simulation of such big systems is still computationally very expensive. Moreover, other probable errors induced by pK_a calculation of some residues cannot be ruled out. Further studies can investigate different protonation states of His172 as an essential determinant of the overall SF configuration and water permeation.

DATA AVAILABILITY STATEMENT

Research data are not shared.

ORCID

Hooman Hadidi  <https://orcid.org/0000-0002-2273-1539>

Reza Kamali  <https://orcid.org/0000-0002-8160-9277>

REFERENCES

- King LS, Kozono D, Agre P. From structure to disease: the evolving tale of aquaporin biology. *Nat Rev Mol Cell Biol.* 2004;5(9):687-698.
- Hub JS, Grubmuller H, de Groot BL. Dynamics and energetics of permeation through aquaporins. What do we learn from molecular dynamics simulations? *Handb Exp Pharmacol.* 2008;190:57-76.
- Lancaster JR. Simulation of the diffusion and reaction of endogenously produced nitric oxide. *Proc Natl Acad Sci.* 1994;91(17):8137-8141.
- Payne JA, Forbush B. Alternatively spliced isoforms of the putative renal Na-K-Cl cotransporter are differentially distributed within the rabbit kidney. *Proc Natl Acad Sci.* 1994;91(10):4544-4548.
- Wang Y, Tajkhorshid E. Nitric oxide conduction by the brain aquaporin AQP4. *Proteins: Struct, Funct, Bioinf.* 2010;78(3):661-670.
- Verkman AS. Aquaporins in clinical medicine. *Annu Rev Med.* 2012;63: 303-316.
- Kreida S, Toernroth-Horsefield S. Structural insights into aquaporin selectivity and regulation. *Curr Opin Struct Biol.* 2015;33:126-134.
- Fischer G et al. Crystal structure of a yeast aquaporin at 1.15 Å reveals a novel gating mechanism. *PLoS Biol.* 2009;7(6):e1000130.
- Törnroth-Horsefield S, Hedfalk K, Fischer G, Lindkvist-Petersson K, Neutze R. Structural insights into eukaryotic aquaporin regulation. *FEBS Lett.* 2010;584(12):2580-2588.
- Janosi L, Ceccarelli M. The gating mechanism of the human aquaporin 5 revealed by molecular dynamics simulations. *PLOS One.* 2013;8(4): e59897.
- Frick A et al. X-ray structure of human aquaporin 2 and its implications for nephrogenic diabetes insipidus and trafficking. *Proc Natl Acad Sci U S A.* 2014;111(17):6305-6310.
- Sui H, Han B-G, Lee JK, Walian P, Jap BK. Structural basis of water-specific transport through the AQP1 water channel. *Nature.* 2001; 414(6866):872-878.
- Murata K, Mitsuoka K, Hirai T, et al. Structural determinants of water permeation through aquaporin-1. *Nature.* 2000;407(6804): 599-605.
- Binesh AR, Kamali R. Molecular dynamics insights into human aquaporin 2 water channel. *Biophys Chem.* 2015;207:107-113.
- Zhu F, Tajkhorshid E, Schulten K. Theory and simulation of water permeation in aquaporin-1. *Biophys J.* 2004;86(1):50-57.
- Hashido M, Ikeguchi M, Kidera A. Comparative simulations of aquaporin family: AQP1, AQPZ, AQP0 and GlpF. *FEBS Lett.* 2005;579 (25):5549-5552.
- Jensen MO, Mouritsen OG. Single-channel water permeabilities of *Escherichia coli* aquaporins AqpZ and GlpF. *Biophys J.* 2006;90(7): 2270-2284.
- Garate JA, English NJ, MacElroy JMD. Human aquaporin 4 gating dynamics in dc and ac electric fields: a molecular dynamics study. *J Chem Phys.* 2011;134(5):055110.
- Xin L, Su H, Nielsen CH, Tang C, Torres J, Mu Y. Water permeation dynamics of AqpZ: a tale of two states. *Biochim Biophys Acta Biomembr.* 2011;1808(6):1581-1586.
- Padhi S, Priyakumar UD. Microsecond simulation of human aquaporin 2 reveals structural determinants of water permeability and selectivity. *Biochim Biophys Acta.* 2017;1859(1):10-16.
- Yamamoto E, Akimoto T, Hirano Y, Yasui M, Yasuoka K. 1/f fluctuations of amino acids regulate water transportation in aquaporin 1. *Phys Rev E.* 2014;89(2):022718.
- Alberga D, Nicolotti O, Lattanzi G, et al. A new gating site in human aquaporin-4: insights from molecular dynamics simulations. *Biochim Biophys Acta.* 2014;1838(12):3052-3060.
- Martínez-Rosell G, Giorgino T, De Fabritiis G. PlayMolecule ProteinPrepare: a web application for protein preparation for molecular dynamics simulations. *J Chem Inf Model.* 2017;57(7):1511-1516.
- Humphrey W, Dalke A, Schulten K. VMD: visual molecular dynamics. *J Mol Graph.* 1996;14(1):33-38.
- Phillips JC, Braun R, Wang W, et al. Scalable molecular dynamics with NAMD. *J Comput Chem.* 2005;26(16):1781-1802.
- Best RB et al. Optimization of the additive CHARMM all-atom protein force field targeting improved sampling of the backbone ϕ , ψ and side-chain χ_1 and χ_2 dihedral angles. *J Chem Theory Comput.* 2012;8 (9):3257-3273.
- Klauda JB, Venable RM, Freites JA, et al. Update of the CHARMM all-atom additive force field for lipids: validation on six lipid types. *J Phys Chem B.* 2010;114(23):7830-7843.
- Jorgensen WL, Chandrasekhar J, Madura JD, Impey RW, Klein ML. Comparison of simple potential functions for simulating liquid water. *J Chem Phys.* 1983;79(2):926-935.
- Feller SE, Zhang Y, Pastor RW, Brooks BR. Constant pressure molecular dynamics simulation: the Langevin piston method. *J Chem Phys.* 1995;103(11):4613-4621.
- Essmann U, Perera L, Berkowitz ML, Darden T, Lee H, Pedersen LG. A smooth particle mesh Ewald method. *J Chem Phys.* 1995;103(19): 8577-8593.
- Berezhkovskii A, Hummer G. Single-file transport of water molecules through a carbon nanotube. *Phys Rev Lett.* 2002;89(6):064503.
- Tajkhorshid E, Zhu F, Schulten K. Kinetic theory and simulation of single-channel water transport. *Handbook of Materials Modeling.* Switzerland AG: Springer; 2005:1797-1822.
- Zhu F, Tajkhorshid E, Schulten K. Collective diffusion model for water permeation through microscopic channels. *Phys Rev Lett.* 2004;93 (22):224501.
- Sasseville LJ, Cuervo JE, Lapointe JY, Noskov SY. The structural pathway for water permeation through sodium-glucose cotransporters. *Biophys J.* 2011;101(8):1887-1895.
- Contreras-Riquelme S, Garate J-A, Perez-Acle T, Martin AJM. RIP-MD: a tool to study residue interaction networks in protein molecular dynamics. *PeerJ.* 2018;6:e5998.
- Wambo TO, Rodriguez RA, Chen LY. Computing osmotic permeabilities of aquaporins AQP4, AQP5, and GlpF from near-equilibrium simulations. *Biochim Biophys Acta Biomembr.* 2017;1859(8):1310-1316.

37. Tong J, Wu Z, Briggs MM, Schulten K, McIntosh TJ. The water permeability and pore entrance structure of aquaporin-4 depend on lipid bilayer thickness. *Biophys J.* 2016;111(1):90-99.
38. Smart OS, Goodfellow JM, Wallace BA. The pore dimensions of gramicidin a. *Biophys J.* 1993;65(6):2455-2460.
39. Grossfield A, Zuckerman DM. Quantifying uncertainty and sampling quality in biomolecular simulations. *Annu Rep Comput Chem.* 2009;5:23-48.
40. Yang B, Verkman AS. Water and glycerol permeabilities of aquaporins 1-5 and MIP determined quantitatively by expression of epitope-tagged constructs inXenopus oocytes. *J Biol Chem.* 1997;272(26):16140-16146.

SUPPORTING INFORMATION

Additional supporting information may be found online in the Supporting Information section at the end of this article.

How to cite this article: Hadidi H, Kamali R, Binesh A. Investigation of the aquaporin-2 gating mechanism with molecular dynamics simulations. *Proteins.* 2021;89:819-831.
<https://doi.org/10.1002/prot.26061>